# 11

# Regge models for many–particle cross–sections

## 11.1 Introduction

In chapter 3 we showed how Regge trajectories could be generated by the imposition of unitarity on the basic exchange force, whether that force was a non-relativistic potential, a single-particle-exchange Feynman diagram in a field theory, or even a single Reggeon-exchange force in a bootstrap model. But the various bootstrap methods which we reviewed in section 3.5 all suffered from the very serious defect that they were limited to two-body unitarity in one channel or another. In chapters 9 and 10 we have found that Regge theory can also predict successfully the sort of behaviour to be expected in many-particle scattering amplitudes, so it is now possible to return to some of the most fundamental questions of Regge theory, such as how the Regge singularities are self-consistent under unitarity, and whether the bootstrap idea introduced in section 2.8 can be correct.

For this purpose we need models for many-particle production processes, and in the next two sections we examine two such models. One, the diffraction model, though inadequate by itself, does describe Pomeron-exchange effects and the fragmentation region, while the other, the multi-peripheral model, though applicable only in certain regions of phase space, allows one to approximate the effect of multi-Reggeon exchange. The so-called 'two-component model' which incorporates both these contributions seems to account quite well for the basic structure of many-particle cross-sections, if not all the details.

The next step is to try and convert this success into a self-consistent bootstrap model combining both duality and unitarity. This is a major task which has certainly not yet been completed satisfactorily. But in the final sections of this chapter we review some of the progress which has been made.
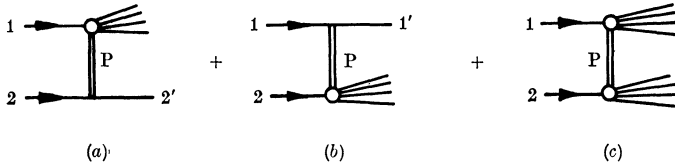
[ 364 ]

FIG. 11.1 The diffraction model in which the incoming particles are excited by P exchange to high-mass 'novae' which subsequently decay into particles.

## 11.2 The diffraction model

This model was proposed by various authors under a variety of names such as 'the diffractive excitation model' (Good and Walker 1960, Adair 1968, Hwa *et al.* 1970, 1971, 1972), 'the limiting fragmentation model' (Benecke *et al.* 1969), 'the fireball' model (Hagedorn 1965, 1970) and 'the nova model' (Jacob and Slansky 1972, Jacob, Berger and Slansky 1972), each with a somewhat different physical motivation. Originally it may have been hoped that the model might account for most of the high energy cross-section, but this is now known not to be true. It does, however, provide a significant fraction ($\approx 20\%$) of the events as we shall see. Our presentation will be based mainly on the nova version (see for example Berger 1971*b*).

The model incorporates the three Pomeron-exchange diagrams of fig. 11.1 in which the incoming particles are excited to form 'novae' or 'fireballs' which then decay into the observed final-state particles. This clearly reproduces the leading-particle effect. The three diagrams are supposed to add incoherently. It is assumed that the inelasticity is small so that rather few particles are produced (which is true, since empirically $\langle n \rangle \propto \log s$), that most particles are produced only with small $p_\mathrm{T}$ (also true – see fig. 10.17), and that only the energy-independent, scaling, single-P exchange is important (which is in fact wrong).

The cross-section for producing a fireball of mass $M$ from particle $i$ is denoted by $\rho_i(M)$, so that the total inelastic cross-section can be written as the sum of figs. 11.1, in the form

$$\sigma_{12}^{\mathrm{in}}(s) = \int_{M_0}^{\sqrt{s}-m_2} \rho_1(M)\,\mathrm{d}M + \int_{M_0}^{\sqrt{s}-m_2} \rho_2(M)\,\mathrm{d}M$$

$$+ \iint_{M_0}^{M_1+M_2=\sqrt{s}} \rho_1(M_1)\,\rho_2(M_2)\,R(M_1,M_2)\,\mathrm{d}M_1\,\mathrm{d}M_2$$

$$\approx \sum_{i=1,2} \int^{\sqrt{s}} \rho_i(M)\,\mathrm{d}M \qquad (11.2.1)$$

if for simplicity we neglect the third term by keeping $R$ small. Here $M_0 \geqslant m_1, m_2$ is the lowest possible mass for a nova, and the upper limit of integration is the approximate kinematical limit required by energy conservation.

If we define $N(M)$ as the average number of particles produced in the decay of a nova of mass $M$, then the average multiplicity in an event will be

$$\langle n \rangle = \sum_i \frac{\displaystyle\int N(M)\rho_i(M)\,\mathrm{d}M}{\displaystyle\int \rho_i(M)\,\mathrm{d}M} = \frac{2\displaystyle\int N(M)\rho(M)\,\mathrm{d}M}{\sigma_{12}^{\mathrm{in}}} \qquad (11.2.2)$$

if the two $\rho_i$ are taken to be identical.

The decay of a nova into, say, pions is described by the function $\mathrm{d}^3D/\mathrm{d}^3\boldsymbol{q}$, giving the probability that a given pion is emitted into the phase-space volume element $\mathrm{d}^3\boldsymbol{q}$ in the nova's rest frame. So the centre-of-mass frame distribution of pions will be (for each nova)

$$\frac{\mathrm{d}^3\sigma}{\mathrm{d}^3\boldsymbol{p}} = \int N(M)\rho(M)\frac{\mathrm{d}^3D}{\mathrm{d}^3\boldsymbol{q}}\left(\frac{\partial^3\boldsymbol{q}}{\partial^3\boldsymbol{p}}\right)\mathrm{d}M \qquad (11.2.3)$$

the last factor being the Jacobian for the Lorentz transformation from the nova's rest frame to the centre-of-mass, a transformation which clearly depends on $M$. So (11.2.3) gives us the pion distribution in terms of three functions, $N$, $\rho$ and $\mathrm{d}^3D/\mathrm{d}^3\boldsymbol{q}$, which have to be determined.

Since we are not concerned with the $p_{\mathrm{T}}$ distribution, which will simply be built into $\mathrm{d}^3D/\mathrm{d}^3\boldsymbol{q}$, and since $q_{\mathrm{T}}$ is unchanged by a Lorentz transformation along the $z$ axis, it is convenient to define

$$A(M, y) \equiv \int \frac{\mathrm{d}^3D}{\mathrm{d}^3\boldsymbol{q}}\left(\frac{\partial^3\boldsymbol{q}}{\partial^3\boldsymbol{p}}\right)\mathrm{d}^2\boldsymbol{p}_{\mathrm{T}} \qquad (11.2.4)$$

and then neglect any transverse motion of the nova so that $\boldsymbol{q}_{\mathrm{T}} = \boldsymbol{p}_{\mathrm{T}}$, which gives

$$\frac{\mathrm{d}\sigma}{\mathrm{d}y} \approx \int^{\sqrt{s}} N(M)\rho(M)A(M, y)\,\mathrm{d}M \qquad (11.2.5)$$

But these approximations are certainly not essential and more exact kinematics can be employed if desired.

It is simplest to assume an isotropic decay of the nova in its rest frame, so one can put

$$\frac{\mathrm{d}^3D}{\mathrm{d}^3\boldsymbol{q}} \propto \mathrm{e}^{-q^2/K^2} = \mathrm{e}^{-(q_{\mathrm{L}}^2 + q_{\mathrm{T}}^2)/K^2} \approx \mathrm{e}^{-q_{\mathrm{L}}^2/K^2}\mathrm{e}^{-p_{\mathrm{T}}^2/K^2} \qquad (11.2.6)$$

where $K$ must be $\approx 0.45\,\mathrm{GeV}/c$ to fit the observed $p_\mathrm{T}$ distribution (see for example fig. 10.17). Then writing (see (10.2.18))

$$q_{3L} = \mu_3 \sinh y_0 \tag{11.2.7}$$

where $y_0$ is the pion's rapidity in the nova's rest frame, and integrating over $q_\mathrm{T}^2$, we get

$$\frac{\mathrm{d}D}{\mathrm{d}y_0} \propto \mathrm{e}^{(\mu_3 \sinh y_0/K)^2} \tag{11.2.8}$$

Now in the centre-of-mass system $y_0$ is boosted to $y = y_0 \pm y_M$, where $y_M$ is the nova's rapidity ($\pm$ for 1, 2 fragmentation), and from (10.2.17) and (10.2.7), neglecting the transverse motion of the nova, we have for fragments of 1,

$$\sinh y_M = \frac{p_{LM}}{M} \approx \frac{p_M}{M} \approx \frac{[s^2 - 2(M^2 + m_2^2)\,s + (M^2 - m_2^2)^2]^{\frac{1}{2}}}{2(\sqrt{s})\,M}$$

$$\underset{M^2 \gg m_2^2}{\approx} \frac{s - M^2}{2(\sqrt{s})\,M} \underset{s \gg M^2}{\approx} \frac{\sqrt{s}}{2M} \tag{11.2.9}$$

and so, since $\sinh y_M \approx \frac{1}{2}\mathrm{e}^{y_M}$ for $y_M \gg 1$, we get

$$y_M \approx \tfrac{1}{2}\log\frac{s}{M^2} \tag{11.2.10}$$

for heavy novae at very high energies.

The mean value of $q_{x,y,z}$ in (11.2.6) is $K$, so the typical energy available to a pion in a nova decay must be

$$Q \approx \sqrt{\tfrac{3}{2}}K \approx 0.5\,\mathrm{GeV} \tag{11.2.11}$$

(neglecting the pion mass) which is in agreement with observation, so if only pions are emitted, the average number produced by a nova of mass $M$ will be

$$N(M) = \gamma(M - M_0) \tag{11.2.12}$$

where $M_0$ is the ground state energy ($= m_{1,2}$ probably), and $\gamma = 1/Q \simeq 2$. However, we want the average multiplicity of pions to increase only slowly with $s$, and to achieve this given (11.2.12) it is essential that the probability of producing high-mass novae be small. In fact if (11.2.12) is inserted in (11.2.2) it is clear that we must have $\rho(M) \sim 1/M^2$ if the average multiplicity is to increase logarithmically, for then

$$\langle n \rangle \to \int^{\sqrt{s}} \gamma\,\frac{\mathrm{d}M}{M} \to \frac{\gamma}{2}\log s \tag{11.2.13}$$

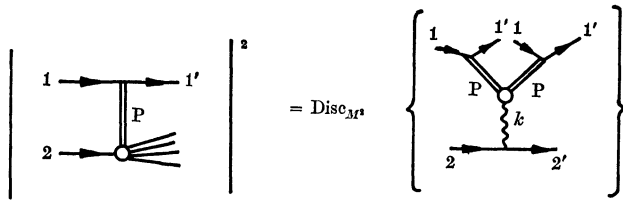So the single empirical constant, $K$, determines the form of the functions $A$, $N$, and $\rho$.

FIG. 11.2   The contribution of fig. 11.1 (*b*) to the Mueller optical theorem; cf. fig. 10.23.

It is interesting to look at these requirements from the Regge viewpoint since for example fig. 11.1 (*b*) gives the cross-section for the inclusive process $1+2 \to 1'+X$, with $M_X = M$, in the triple-Regge region $x_1 \approx 1$, so that (see fig. 11.2)

$$\rho_2(M) = \int_{-\infty}^{0} \frac{\mathrm{d}^2\sigma}{\mathrm{d}t\,\mathrm{d}M} \,\mathrm{d}t = \int_{-\infty}^{0} \frac{2M\mathrm{d}^2\sigma}{\mathrm{d}t\,\mathrm{d}M^2}\,\mathrm{d}t$$

$$= \sum_k \frac{1}{16\pi^2} \int_{-\infty}^{0} G_{11,\,2}^{\mathrm{PP};\,k}(t)\, s^{2\alpha_{\mathrm{P}}(t)-2}\, 2(M^2)^{\alpha_k(0)-2\alpha_{\mathrm{P}}(t)+\frac{1}{2}}\,\mathrm{d}t$$

$$(11.2.14)$$

from (10.8.6). The dominant region of the $t$ integration will be $t \approx 0$, since $G(t)$ falls exponentially with $-t$, where $\alpha_{\mathrm{P}}(t) \approx 1$. The leading trajectory $k$ should be the Pomeron, but $\alpha_k(0) = 1$ gives too slow a fall of (11.2.14) with $M^2$. However, we can perhaps neglect this term on the grounds that the triple-Pomeron coupling is small (remembering also that a finite $\gamma^{\mathrm{PP},\,\mathrm{P}}(t=0)$ is not self-consistent, at least in the pole approximation which we are employing) so that for moderate values of $M^2$ the dominant contribution will be $k = \mathrm{R}(= \rho, \omega, \mathrm{A}_2, \mathrm{f})$ with $\alpha_{\mathrm{R}}(0) \approx 0.5$, giving

$$\rho_2(M) \sim \frac{1}{M^2} \qquad (11.2.15)$$

So from this point of view it looks as though the model may work for intermediate $M^2$, but not large $M^2$, though we must also remember that $M^2 \to s$ takes us outside the triple-Regge Region.

Jacob *et al.* (1972) used the parameterization

$$\rho_i(M) = C_i \frac{\mathrm{e}^{-\beta_i/(M-m_i)}}{(M-m_i)^2}, \quad i = 1, 2 \qquad (11.2.16)$$

which has the required $M^{-2}$ asymptotic behaviour, with a peak at $M = m_i + \frac{1}{2}\beta_i$; $C_1$ and $\beta_i$ are free parameters to be adjusted to fit the data on $\sigma_{12}^{\mathrm{in}}$, the inclusive distributions, etc.
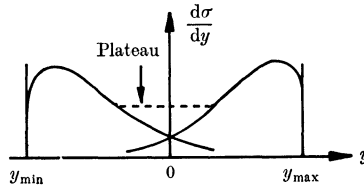
FIG. 11.3    The tails of the two nova distributions produce a central plateau in rapidity.

It is possible to reproduce the inclusive distributions, with their flat central plateau, only because of the $M^{-2}$ tail of $\rho(M)$. From (11.2.8), since $y = y_0 \pm y_M$, the central region $y \approx 0$ requires $y_M \approx 0$, which from (11.2.9) means $M \approx \sqrt{s}$. So this region is occupied by novae which are as heavy as energy conservation permits. Since $\rho(M)\,N(M) \sim M^{-1}$ there is a finite contribution from this region of integration in (11.2.5) and so a central plateau can develop as in fig. 11.3.

Since, from (11.2.2), (11.2.13),

$$\langle n \rangle = \frac{\int \dfrac{\mathrm{d}\sigma}{\mathrm{d}y}\,\mathrm{d}y}{\sigma_{12}^{\mathrm{in}}} \to \frac{\gamma}{2}\log s \qquad (11.2.17)$$

we have

$$\frac{1}{\sigma_{12}^{\mathrm{in}}}\frac{\mathrm{d}\sigma}{\mathrm{d}y}\bigg|_{\mathrm{plateau}} \approx \frac{\gamma}{2} \approx 1$$

which is compatible with the data to within a factor of 2.

Of course the third term of fig. 11.1 may also be included, and is regarded by some authors (e.g. Hwa) as the most important, and by others as at least equally important at high energies. However, since even with such modifications the model is unable to account for many of the crucial features of many-particle production we shall not pursue these variants here.

The first problem concerns particle correlations. From (10.3.4) and (11.2.2) we obtain with (11.2.12) and (11.2.15)

$$\langle n(n-1) \rangle = 2 \int \frac{N(M)\,(N(M)-1)\,\rho(M)\,\mathrm{d}M}{\sigma_{12}^{\mathrm{in}}} \underset{s\to\infty}{\sim} \int^{\sqrt{s}} \mathrm{d}M \to \sqrt{s} \qquad (11.2.18)$$

so, even though $F_1 \sim \log s$, $F_2 \sim \sqrt{s}$ and hence from (10.10.4) $C_2 \sim \sqrt{s}$ as well. In fact it is obvious that the model predicts

$$C_n \sim F_n \sim (\sqrt{s})^{n-1}, \quad n > 1 \qquad (11.2.19)$$

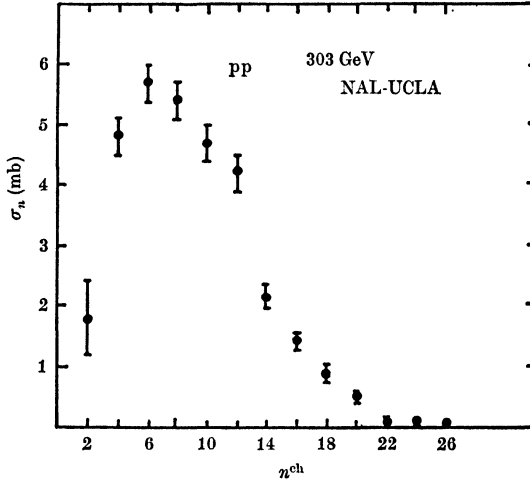which is incompatible with the high energy data (e.g. fig. 10.29).

FIG 11.4   Date for $\sigma_n$ against $n$ at fixed $s$ for charged particles.

Also, since $\rho(M) \sim M^{-2}$ and $N(M) \sim M$, the cross-section for producing $n$ particles, $\sigma_n(s)$, has the behaviour for large $n$, at fixed $s$,

$$\sigma_n(s) \xrightarrow[n \to \infty]{} \frac{d\sigma_{12}^{in}}{dn} \propto \frac{d\sigma_{12}^{in}}{dM} \sim \frac{1}{M^2} \sim \frac{1}{n^2} \qquad (11.2.20)$$

from (11.2.1). But experimentally (fig. 11.4) it is falling much faster than this for large $n$. Part of the problem could be just the failure of this simple version of the model to take into account the phase-space restrictions on producing large numbers of particles, but it has been shown by Le Bellac and Meunier (1973) that even using proper kinematics it is not possible to fit simultaneously the flat $d\sigma/dy$ for $y \approx 0$ and $\sigma_n$.

If we include the triple-Pomeron term in (11.2.14) for large $M^2$, then clearly $N(M) \propto M$ is impossible if we also wish to retain $\langle n \rangle \sim \log s$. If we regard the Pomeron as an ordinary particle then fig. 11.1 (b) is just the process $P_v + 2 \to X$ where $P_v$ is the virtual Pomeron, and as $M$ is the total energy for this process we would expect

$$\langle n \rangle \approx C \log (M^2) \qquad (11.2.21)$$

where $C$ is some constant, which seems to be true experimentally (fig. 11.5). Then $dn = 2C\, dM/M$ and so for large $n$

$$\sigma_n(s) \xrightarrow[n \to \infty]{} \frac{d\sigma_{12}^{in}}{dn} \propto M \frac{d\sigma}{dM} = 2M^2 \frac{d\sigma}{dM^2} = \int_{-\infty}^{0} 2M^2 \frac{d^2\sigma}{dt\, dM^2}\, dt \qquad (11.2.22)$$
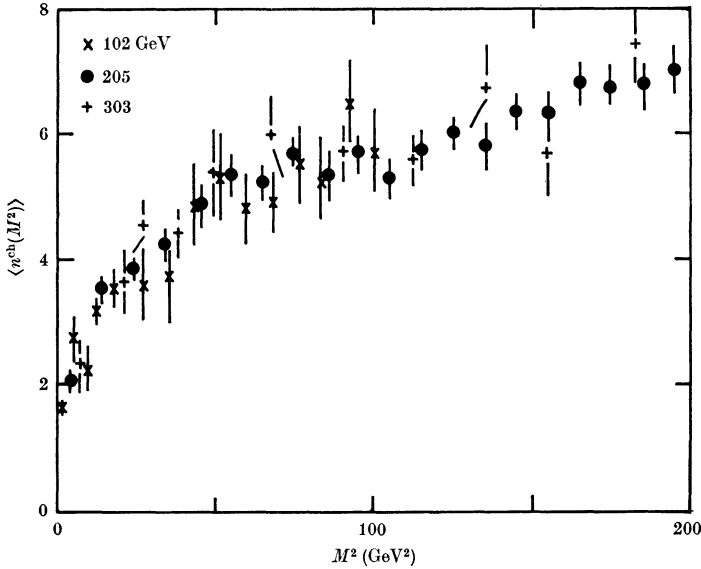
FIG. 11.5   The mean number of charged particles produced in $pp \to pX$ as a function of $M^2$ at various energies. This is consistent with the form

$$\langle n \rangle = B + C \log (M^2).$$

(From Fox 1973.)

so using (10.8.6) with $G_{11,\,2}^{\mathrm{PP;P}}(t) \propto \mathrm{e}^{at}$ and $\alpha_{\mathrm{P}}(t) = 1 + \alpha_{\mathrm{P}}' t$ we find

$$\sigma_n \propto \left(a + 2\alpha_{\mathrm{P}}' \log \left(s - \frac{n}{c}\right)\right)^{-1} \qquad (11.2.23)$$

So each $\sigma_n \sim (\log s)^{-1}$ even though

$$\langle n \rangle \propto \int n \sigma_n \, \mathrm{d}n \propto \log s$$

Alternatively, with a vanishing triple-Pomeron coupling,

$$G_{11,\,2}^{\mathrm{PP;P}}(t) \propto (-t) \, \mathrm{e}^{at}$$

we get                    $$\sigma_n \propto \left(a + 2\alpha_{\mathrm{P}}' \log \left(s - \frac{n}{c}\right)\right)^{-2} \qquad (11.2.24)$$

These results are like those of the multi-peripheral model, to be described in the next section, and it is clear that P exchange cannot give a consistent view of $\sigma_n$ versus $n$. So, even bearing in mind the fact that the triple-Regge formation is strictly applicable only for $M^2/s \ll 1$, this does appear to help us to understand why the nova model is incorrect.
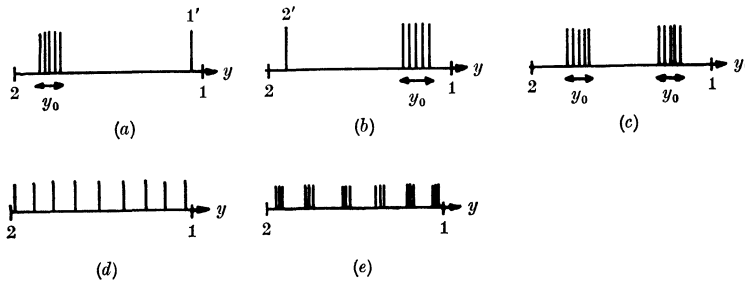
13                                                                CIT

FIG. 11.6   Rapidity distributions: Diagram (a) corresponds to fig. 11.1 (b) in which 1′ has a rapidity close to that of 1, while the fragments of 2 are clustered within a length $y_0$. Similarly, (b) corresponds to fig. 11.1 (a) and (c) to 11.1 (c). (d) The rapidity distribution in the multi-peripheral model. (e) The rapidity distribution for clusters produced multi-peripherally.

But perhaps the most serious defect of the diffraction model from an experimental viewpoint is that a given diffractive event is predicted to have a rapidity distribution like fig. 11.6 (a), (b) or (c), with a large gap between the fragments of 1 and those of 2, the fragments being clustered within a range $y_0$ (see (11.2.8)), even though, when one averages over a large number of events, a flat rapidity distribution may be obtained. In fact only a fraction of the observed events have this structure, many more having the more uniform distribution characteristic of the multi-peripheral model (fig. 11.6 (d), (e)).

So it is clear that the diffraction model can at best account for only a small part of the high energy cross-section. In section 11.6 we shall combine this diffractive P contribution with the more dominant multi-peripheral amplitude.

## 11.3   The multi-peripheral model

The basic idea behind the multi-peripheral model is that at high energy the dominant production mechanism should be like fig. 11.7, in which each particle along the chain is produced peripherally, i.e. at small momentum transfer with respect to those adjacent to it. The original version (Bertocchi, Fubini and Tonin 1962, Amati *et al.* 1962 *a, b*) often referred to as 'the ABFST model' after the initials of the authors, involved elementary pion exchange between successive particles, but we should now think it more appropriate to use Reggeon exchanges instead (Chew *et al.* 1968, 1969, 1970, Halliday 1969, Halliday and Saunders 1969, de Tar 1971), and we might eventually want to include Regge cuts as well.
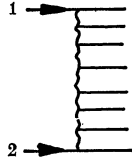
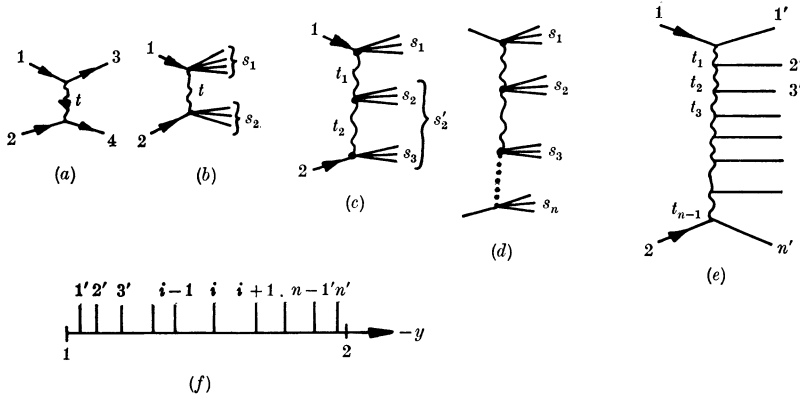FIG. 11.7  The multi-peripheral model with Reggeon exchanges.



FIG. 11.8  (a) Peripheral exchange in $2 \to 2$ scattering. (b) Peripheral $2 \to n$ amplitude. (c) Doubly peripheral process. (d) Multi-peripheral process. (e) Multi-peripheral production of single particles, $1 + 2 \to 1' + 2' + \ldots + n'$. (f) Strong ordering which occurs when the ordering of the particles in rapidity is the same as the ordering of their couplings, i.e. the same as in (e).

A two-body amplitude like fig. 11.8(a) can often be represented at fixed $s$ by (cf. (6.8.11))

$$A(s, t) \propto e^{ct} \tag{11.3.1}$$

with $c \approx 2$–$6\,\text{GeV}^{-2}$, indicating the dominance of low-$t$ singularities, i.e. the longer range forces, so that as discussed in section 2.4 the beam can be thought of as interacting strongly with the periphery of the target, and the amplitude is rapidly damped in $t$. So we can regard an interaction as peripheral, in this sense, if say $|t| \leqslant \tau \equiv 0.5\,\text{GeV}^2$ includes the bulk of the events. (The reader should note that this is a somewhat different use of 'peripheral' from that of section 8.6 where the word meant dominance of impact parameter $b \approx R = 1\,\text{fm}$, producing $t$ dependence of the form $J_n(R\sqrt{-t})$. It is rather unfortunate that both meanings of the word are in current use.)

Similarly the many-particle amplitude, fig. 11.8(b), is said to be peripheral if $|t| \leqslant \tau$, and we can expect this to be the dominant $t$-region for $s \gg s_1, s_2$. However, the minimum possible value of $|t|$,

13-2

i.e. $|t_{\min}|$, is determined by the kinematics and depends on $s_1$ and $s_2$. From (1.7.17) we have, replacing $m_3^2$ and $m_4^2$ by $s_1$ and $s_2$ respectively,

$$z_s = \frac{s^2 + s(2t - \Sigma) + (m_1^2 - m_2^2)(s_1 - s_2)}{\{[s - (m_1 + m_2)^2][s - (m_1 - m_2)^2][s - (\sqrt{s_1} + \sqrt{s_2})^2][s - (\sqrt{s_1} - \sqrt{s_2})^2]\}^{\frac{1}{2}}}$$

(11.3.2)

$$\Sigma \equiv m_1^2 + m_2^2 + s_1 + s_2$$

So taking $s, s_1, s_2 \gg m_1^2, m_2^2$ this gives

$$z_s \approx \frac{s + 2t - s_1 - s_2}{\{[s - (\sqrt{s_1} + \sqrt{s_2})^2][s - (\sqrt{s_1} - \sqrt{s_2})^2]\}^{\frac{1}{2}}}$$

(11.3.3)

and for $s \gg t, s_1, s_2$ the forward direction, $z_s = 1$, is given by

$$t = t_{\min} \approx -\frac{s_1 s_2}{s}$$

(11.3.4)

(Note that for this $s$-channel process physical $t < 0$, so $t_{\min} \equiv -|t|_{\min}$ is in fact the maximum possible value of $t$.) Therefore the process in fig. 11.8(b) can only be peripheral if $|t_{\min}| \leqslant \tau$, i.e. if

$$\frac{s_1 s_2}{s} \leqslant \tau,$$

(11.3.5)

which corresponds to the single-Regge limit of section 9.3.

Extending this idea, a process can be doubly peripheral, like fig. 11.8(c) if

$$|t_{1\min}| = \frac{s_1 s_2'}{s} \leqslant \tau \quad \text{and} \quad |t_{2\min}| = \frac{s_2 s_3}{s_2'} \leqslant \tau$$

(11.3.6)

and so

$$\frac{s_1 s_2'}{s} \cdot \frac{s_2 s_3}{s_2'} = \frac{s_1 s_2 s_3}{s} \leqslant \tau^2$$

(11.3.7)

Note that because of the way we have chosen to analyse the diagram $s_2'$ is the energy appropriate to $t_2$ exchange, not $s$, but the final result (11.3.7) treats $s_1 s_2 s_3$ symmetrically. And for $n$ clusters, fig. 11.8(d), we need

$$\frac{s_1 s_2 \dots s_n}{s} \leqslant \tau^{n-1}$$

(11.3.8)

An immediate consequence of this hypothesis is that if we suppose all the clusters to have some average mass, so $\langle s_i \rangle = s_A$, say, $i = 1, \dots, n$ then (11.3.7) gives

$$\frac{s_A^{\langle n \rangle}}{s} \leqslant \tau^{\langle n \rangle - 1}$$

(11.3.9)

where $\langle n \rangle$ is the average number of clusters produced, and so

$$\langle n \rangle \log s_{\mathrm{A}} - \log s \leqslant (\langle n \rangle - 1) \log \tau$$

or
$$\langle n \rangle \leqslant \log \left( \frac{s}{\tau} \right) \log \left( \frac{\tau}{s_{\mathrm{A}}} \right) \tag{11.3.10}$$

So the average number of clusters increases at most logarithmically with $s$, an experimentally desirable result, particularly if we take the 'clusters' to be single particles, as in fig. 11.8(e).

In this case we can write a multi-peripheral model for the amplitude $1 + 2 \rightarrow 1' + \ldots + n'$ in the form suggested by the multi-Regge model (9.3.10):

$$A^{2 \rightarrow n}(p_1, p_2; p_1', \ldots, p_n') = \gamma(t_1) R(t_1, s_{12}) G(t_1, t_2, \eta_{12})$$
$$\times R(t_2, s_{23}) G(t_2, t_3, \eta_{12}) \ldots R(t_{n-1}, s_{n-1,n}) \gamma(t_{n-1}) \tag{11.3.11}$$

where the $\gamma$'s and $G$'s are the couplings and

$$R(t_i, s_{i,i+1}) \equiv R_i \tag{11.3.12}$$

represents the $i$th Reggeon exchange. Except at the ends the couplings depend both on the Reggeon masses $t_i, t_{i+1}$ and on the Toller angle variable (9.2.31),

$$\eta_{i,i+1} = \frac{s_{i,i+1,i+2}}{s_{i,i+1} s_{i+1,i+2}} \tag{11.3.13}$$

Clearly we have assumed factorization in writing (11.3.11) as well as multiperipherality. The equation is rather complicated because of the signature properties of the Reggeons. The simplest version of the model with an elementary scalar-particle-exchange amplitude would just have all $\gamma$'s and $G$'s $= g$, the coupling strength, and $R_i = 1/(t - m_i^2)$, corresponding to the Feynman rules of section 1.12.

Equation (11.3.11) may be approximately valid for $|t_i| \leqslant \tau$, $s_{i,i+1} \gg s_0$ for $i = 1, \ldots, (n-1)$, but this is only a small part of the available phase space, and as discussed in section 9.2 many events will probably have low sub-energies, due for example to resonance production. So to apply the model more widely, as we shall do below, it is necessary to make some sort of duality assumption, that this high-sub-energy form of the amplitude also applies, at least in some average sense, for low $s_{i,i+1}$ as well.

If we assume that the model is approximately valid for all phase space, from (1.8.5) we can calculate the cross-section for producing $n$ particles as

$$\sigma_n \equiv \sigma_{12 \rightarrow n} \approx \frac{1}{2s} \int \mathrm{d}\Phi_n \, |A^{2 \rightarrow n}|^2 \tag{11.3.14}$$

where $d\Phi_n$ is the $n$-particle phase-space volume element of (1.8.6). If we work in the rest frame of particle 1 we can write (see Halliday and Saunders 1969)

$$\left.\begin{array}{l} p_1 = (m_1, 0, 0, 0) \\ p_2 = (m_2 \cosh Y, 0, 0, m_2 \sinh Y) \end{array}\right\} \tag{11.3.15}$$

where (see (10.2.22))

$$Y \equiv y_2 - y_1 \xrightarrow[s\to\infty]{} \log \frac{s}{m_1 m_2} \tag{11.3.16}$$

and for the final-state particles (see (10.2.18))

$$p_i' = (\mu_i \cosh y_i, \boldsymbol{p}_{i\mathrm{T}}, \mu_i \sinh y_i) \tag{11.3.17}$$

Then from (1.8.6) and (10.3.5)

$$d\Phi_n = \prod_{i=1}^{n} \left(\frac{d^2\boldsymbol{p}_{i\mathrm{T}}\, dy_i}{16\pi^3}\right) (2\pi)^2 \delta^2 \left(\sum_{i=1}^{n} \boldsymbol{p}_{i\mathrm{T}}\right) \tfrac{1}{2} 2\pi\delta \left(\sum_{i=1}^{n} \mu_i \mathrm{e}^{y_i} - m_1 - m_2 \mathrm{e}^{Y}\right)$$

$$\times 2\pi\,\delta \left(\sum_{i=1}^{n} \mu_i \mathrm{e}^{-y_i} - m_1 - m_2 \mathrm{e}^{-Y}\right) \tag{11.3.18}$$

To simplify we approximate the Reggeon amplitude by

$$\gamma_i R_i \approx g(s_{i,i+1})^{\alpha} \tag{11.3.19}$$

completely ignoring the dependence of the $\gamma$'s, $G$'s and $\alpha$'s on the $t_i$, and on the Toller angles (11.3.13), and so (11.3.11) becomes

$$A^{2\to n} \approx g^n \prod_{i=1}^{n-1} (s_{i,i+1})^{\alpha} \tag{11.3.20}$$

Now
$$s_{i,i+1} \equiv (p_i' + p_{i+1}')^2 \approx \mu_i \mu_{i+1} \mathrm{e}^{y_{i+1} - y_i} \tag{11.3.21}$$

(see (10.2.22)) and if each $s_{i,i+1}$ is large then $y_{i+1} \gg y_i$ for all $i$. In this region of phase space we have what is called 'strong ordering' in rapidity, i.e. the ordering of the particles in rapidity, fig. 11.8($f$), corresponds exactly to the ordering of their couplings in fig. 11.8($e$), but clearly this is true only in part of phase space. Then

$$\prod_{i=1}^{n-1} s_{i,i+1} = \mu_1 \mu_2^2 \ldots \mu_{n-1}^2 \mu_n \mathrm{e}^{y_n - y_1} \tag{11.3.22}$$

and the maximum contribution in the integral over (11.3.18) comes from $\boldsymbol{p}_{i\mathrm{T}}^2 \approx 0$, so (from (10.2.2)) $\mu_i^2 \approx m_i^2 = m^2$ if we take all the particles

$1', \ldots, n'$ to have the same mass. Hence

$$A^{2 \to n} \approx g^n [(m^2)^{n-2} \mu_1 \mu_n \, e^{y_n - y_1}]^\alpha \qquad (11.3.23)$$

From the $\delta$ functions (11.3.18) we need

$$\mu_1 e^{-y_1} \approx m_1 \quad \text{and} \quad \mu_n e^{y_n} \approx m_2 e^Y$$

(remember $y_{i+1} \gg y_i$ for all $i$ so all the other terms in the $\delta$ functions can be ignored) and hence

$$A^{2 \to n} \approx g^n [(m^2)^{n-2} m_1 m_2 e^Y]^\alpha = g^n [(m^2)^{n-2} s]^\alpha \qquad (11.3.24)$$

from (11.3.16). So our approximations have eliminated all the dependence of $A^{2 \to n}$ on the sub-energies and momentum transfers.

Then putting

$$z_i = y_{i+1} - y_i \qquad (11.3.25)$$

and ignoring $\boldsymbol{p}_{i\mathrm{T}}$ in (11.3.18) we get after some manipulation

$$d\Phi_n \propto \frac{e^{-Y}}{2m_1 m_2} \prod_{i=1}^{n-1} dz_i \, \delta\left(Y - \sum_{i=1}^{n-1} z_i\right) \qquad (11.3.26)$$

and so

$$\sigma_n \propto g^{2n} s^{2\alpha - 2} \int_0^Y \prod_{i=1}^{n-1} dz_i \, \delta\left(Y - \sum_{i=1}^{n-1} z_i\right) \qquad (11.3.27)$$

Now from the Feynman relation (1.12.4)

$$\int_0^1 d\alpha_1 \ldots d\alpha_n \, \delta(\Sigma\alpha - 1) = \frac{1}{(n-1)!}$$

and substituting $\alpha_i = z_i/Y$ we get

$$\int_0^Y dz_i \ldots dz_{n-1} \, \delta(\Sigma z_i - Y) = \frac{Y^{n-2}}{(n-2)!} \qquad (11.3.28)$$

So replacing $g$ by $\bar{g}$, the average of $g$ over the phase-space integration, we obtain

$$\sigma_n = s^{2\alpha - 2} \bar{g}^4 \frac{(\bar{g}^2 Y)^{n-2}}{(n-2)!} \qquad (11.3.29)$$

and hence

$$\sigma_{12}^{\text{tot}} = \sum_n \sigma_n = \sum_{n=2}^\infty s^{2\alpha - 2} \bar{g}^4 \frac{(\bar{g}^2 Y)^{n-2}}{(n-2)!} = \bar{g}^4 e^{Y(2\alpha - 2 + \bar{g}^2)} \qquad (11.3.30)$$

So to get a constant total cross-section we need

$$2\alpha - 2 + \bar{g}^2 = 0, \quad \text{i.e.} \quad \alpha = 1 - \frac{\bar{g}^2}{2} \qquad (11.3.31)$$

Hence $\alpha < 1$, and the amplitude cannot be dominated by multiple P

exchange. Successive P exchange would give $\sigma_n \sim (\log s)^{n-2}$ and $\sigma_{12}^{tot} \sim s^{\bar{g}^2}$ in violation of the Froissart bound (Finkelstein and Kajantie 1968 $a, b$).

If (11.3.31) is substituted back into (11.3.29) we find ($Y = \log s$)

$$\sigma_n = \bar{g}^4 \frac{(\bar{g}^2 Y)^{n-2}}{(n-2)!} e^{-\bar{g}^2 Y} \qquad (11.3.32)$$

so

$$\langle n \rangle = \frac{\sum\limits_n n \sigma_n}{\sum\limits_n \sigma_n} = \bar{g}^2 Y \sim (2 - 2\alpha) \log s \qquad (11.3.33)$$

which gives the required logarithmic increase of the average multiplicity with $s$ (Chew and Pignotti 1968). In fact this result does not really depend in any important way on the details of the model. For if we put say (see Fubini 1963)

$$\sigma_2 = \lambda \bar{\sigma}_2 \qquad (11.3.34)$$

where $\lambda$ is some variable coupling parameter (for example $\lambda =$ the coupling $g^2$), then by factorization (see fig. 11.9),

$$\sigma_n = \lambda^n \bar{\sigma}_n \qquad (11.3.35)$$

so

$$\langle n \rangle = \frac{\sum\limits_n n \lambda^n \bar{\sigma}_n}{\sum\limits_n \lambda^n \bar{\sigma}_n} = \lambda \frac{\mathrm{d}\sigma/\mathrm{d}\lambda}{\sigma} \Bigg|_{\lambda=1} \qquad (11.3.36)$$

Hence if

$$\sigma(s) = \beta(\lambda) s^{\alpha(\lambda)} = e^{\alpha(\lambda)\log s + \beta(\lambda)} \qquad (11.3.37)$$

where $\alpha, \beta$ are arbitrary functions of $\lambda$, then

$$\langle n \rangle = \left( \lambda \frac{\mathrm{d}\alpha}{\mathrm{d}\lambda} \right) \log s + \lambda \frac{\mathrm{d}\beta}{\mathrm{d}\lambda} \Bigg|_{\lambda=1} \qquad (11.3.38)$$

Thus so long as there is some (unspecified) dynamical relation between the power behaviour of $\sigma(s)$ and the magnitude of some factorizable coupling strength we shall always find

$$\langle n \rangle \sim \log s \qquad (11.3.39)$$

independent of the details of the model.

Putting (11.3.33) into (11.3.32) gives

$$\sigma_n = \bar{g}^4 \frac{\langle n \rangle^{n-2} e^{-\langle n \rangle}}{(n-2)!} \qquad (11.3.40)$$

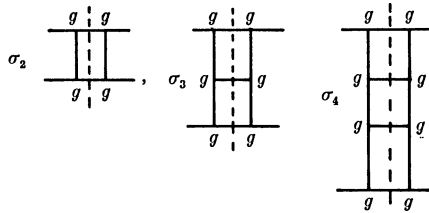so, at fixed $s$, $\sigma_n$ against $n$ has a Poisson distribution whose width

FIG. 11.9 The discontinuities which give the various many-particle cross-sections in the multi-peripheral model. Each successive term contains a factor $g^2$ relative to previous one.

increases like $\log s$. And the average spacing of the particles in rapidity is

$$\Delta y = \frac{Y}{\langle n \rangle} = \frac{1}{\bar{g}^2} \tag{11.3.41}$$

from (11.3.33).

The probability that the $i$th particle has rapidity $y = y_i = \sum_{j=1}^{i-1} z_j$ is

$$\frac{\mathrm{d}\sigma_{n,i}}{\mathrm{d}y} = \mathrm{e}^{Y(2\alpha-2)} \bar{g}^{2n} \int_0^Y \prod_{j=2}^{n-1} \mathrm{d}z_j \, \delta\left(Y - \sum_{j=1}^{n-1} z_j\right) \delta\left(y - \sum_{j=1}^{i-1} z_j\right)$$

$$= \mathrm{e}^{Y(2\alpha-2)} \bar{g}^{2n} \frac{(y)^{i-1}}{(i-1)!} \frac{(Y-y)^{n-i-2}}{(n-i-2)!} \tag{11.3.42}$$

from (11.3.28), the first part coming from the $i-1$ particles with $y < y_i$ and the second from the $n-i$ particles with $y_i < y < Y$, as in fig. 11.8($f$). This distribution is shown in fig. 11.10. So the full inclusive distribution is

$$\frac{\mathrm{d}\sigma}{\mathrm{d}y} = \sum_{i=1}^{n-2} \sum_{n=3}^{\infty} \frac{\mathrm{d}\sigma_{n,i}}{\mathrm{d}y} = \sum_{n=3}^{\infty} \mathrm{e}^{Y(2\alpha-2)} \bar{g}^{2n} \frac{Y^{n-3}}{(n-3)!} \tag{11.3.43}$$

since the binomial expansion gives

$$\frac{Y^{n-3}}{(n-3)!} = \frac{(Y-y+y)^{n-3}}{(n-3)!} = \sum_{i=1}^{n-2} \frac{(Y-y)^{n-i-2}(y)^{i-1}}{(n-i-2)!(i-1)!},$$

and so

$$\frac{\mathrm{d}\sigma}{\mathrm{d}y} = \bar{g}^6 s^{2\alpha-2+g^2} = \bar{g}^6 \tag{11.3.44}$$

if (11.3.31) holds to give $\sigma_{12}^{\mathrm{to}}(s) \to \bar{g}^4$. And so we get a flat, uniform scaling distribution of particles in the central region. And combining (11.3.30) with (11.3.41)

$$\frac{1}{\sigma_{12}^{\mathrm{tot}}} \frac{\mathrm{d}\sigma}{\mathrm{d}y} = \bar{g}^2 = \frac{\langle n \rangle}{\log s} \tag{11.3.45}$$

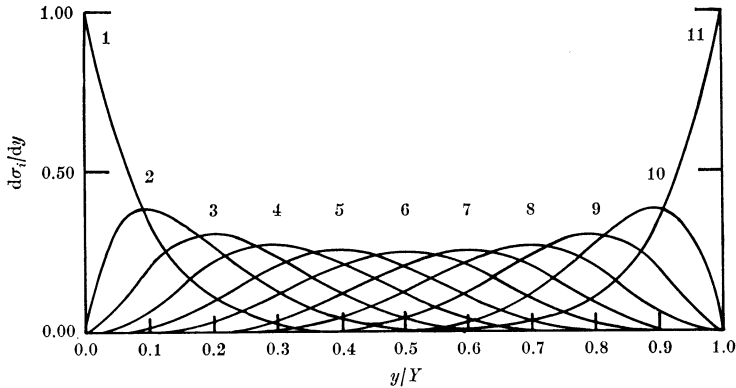which is the same as the diffraction model result (11.2.17). Of course,

FIG. 11.10   The rapidity distribution of the $i$th produced particle $d\sigma_i/dy$ (in arbitrary units) in the multi-peripheral model, for 11 produced particles. From de Tar (1971).

since the amount of rapidity available is increasing like $\log s$, any model with a scaling central distribution and $\langle n \rangle \sim \log s$ must obey (11.3.45).

Similarly one can evaluate $d^2\sigma/dy_i\,dy_i$, and it is found, not surprisingly, that there are no correlations between the produced particles in this factorizing model. We shall show this more simply in section 11.5 below.

The most obvious defect of the model is that it does not give any leading-particle effect, i.e. there is no special enhancement of the probability distribution for particles having a similar rapidity to that of the beam or target particles, which the diffraction model produces so naturally. So in section 11.6 we shall attempt to combine the two models. However, first it is useful to examine the internal self-consistency of the multi-peripheral model.

## 11.4   The multi-peripheral bootstrap

In writing the multi-Regge form for the multi-peripheral amplitude (11.3.11) we can insert arbitrary Regge poles, $\alpha_R$. And then in 'squaring' the amplitude in (11.3.14), and summing over $n$ we obtain the behaviour (11.3.30) for the total cross-section. Thus in (11.3.31) we obtained the condition on the trajectory for constancy of the total cross-section. But obviously this is not self-consistent because a constant $\sigma^{tot}(s)$ requires P exchange with $\alpha_R(0) = 1$, whereas (11.3.31)

demands

$$\alpha_{\mathrm{R}}(0) = 1 - \frac{\bar{g}^2}{2} < 1 \tag{11.4.1}$$

Instead we could demand self-consistency of the input and output Reggeons and require, comparing (6.8.4) and (11.3.30),

$$\sigma_{12}^{\mathrm{tot}}(s) \sim s^{\alpha-1} = \sum_n \sigma_n \sim s^{2\alpha-2-\bar{g}^2} \tag{11.4.2}$$

and so (Chew and Pignotti 1968)

$$\alpha(0) = 1 - \bar{g}^2 < 1 \tag{11.4.3}$$

This is a simple example of a bootstrap calculation. The input Reggeons in the multi-peripheral chain are used in the unitarity equation to build up ladders (see fig. 11.11) which, when summed, give back a Reggeon; and this should, for self-consistency, be identical with the input Reggeons. It is clear from the outset, however, that this can be, at best, only an approximation, because for complete self-consistency we should include cuts in the multi-peripheral chains, and consider diagrams with crossed rungs which give back cuts in the output as well. We shall reconsider this problem in the final section. But here we want to examine a bit more closely the pole-dominance approximation, and so we shall stick to the strong ordering of (11.3.21) *et seq.* with no crossing rungs.

If we adopt the Regge exchange model (11.3.11) for all $2 \to n$ amplitudes, the discontinuity across the two-particle cut (fig. 11.12(b)) is given by (cf. (8.2.11))

$$D_2(s,t) = \frac{1}{16\pi^2 s} \int \int_{-\infty}^{0} \frac{\mathrm{d}t_1 \, \mathrm{d}t_1' \, \theta(-\lambda)}{(-\lambda(t,t_1,t_1'))^{\frac{1}{2}}} \, \gamma^2(t_1) \, R(t_1,s) \, \gamma^{*2}(t_1') \, R^*(t_1',s) \tag{11.4.4}$$

(say) and the complete $s$-channel discontinuity equation of fig. 11.12 is

$$D(s,t) = \sum_{n=2}^{\infty} D_n(s,t) = D_2(s,t) + \sum_{n=3}^{\infty} \int \mathrm{d}\Phi_n \gamma(t_1) \, RGR \ldots \gamma(t_{n-1})$$
$$\times \gamma^*(t_1') \, R^*G^*R^* \ldots \gamma^*(t_{n-1}') \tag{11.4.5}$$

Since this infinite sum involves repetition of the same basic two-Reggeon exchange contribution we can rewrite it recursively (cf. (1.13.27), (3.4.20)), as in fig. 11.12(f), in the form (see Chew *et al.* 1969, Goldberger 1969)

$$D(s,t) = D_2(s,t) + D_2 \otimes D \tag{11.4.6}$$

where $\otimes$ implies integration over $t_2$, $t_2'$ in a similar fashion to (11.4.4). Strictly $D_2$ and $D$ in this integration may be expected to depend on
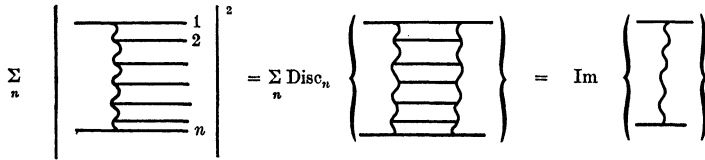
FIG. 11.11   Multi-peripheral bootstrap for a Regge trajectory.

$t_2, t_2'$ but for simplicity we ignore any such dependence here. This integration is simplified if we project into $t$-channel partial waves, defining (from (2.5.3))

$$\left.\begin{aligned} A_2(J,t) &= \frac{1}{16\pi^2} \int^\infty D_2(s,t)\, Q_J(z_t)\, \mathrm{d}s \\ A(J,t) &= \frac{1}{16\pi^2} \int^\infty D(s,t)\, Q_J(z_t)\, \mathrm{d}s \end{aligned}\right\} \tag{11.4.7}$$

and (11.4.6) becomes (cf. (2.2.7))

$$A(J,t) = A_2(J,t) + A_2(J,t)\, A(J,t)$$

or

$$A(J,t) = \frac{A_2(J,t)}{1 - A_2(J,t)} \tag{11.4.8}$$

which gives $A(J,t)$ in terms of $A_2(J,t)$ (provided we accept the drastic approximations made en route). Note that we are using $t$-channel partial waves in the $s$-channel physical region, so really this is an $O(2,1)$ not an $O(3)$ projection (see section 6.6).

A rather disturbing feature of fig. 11.12(b), and (11.4.4), is that they clearly generate an AFS cut (8.2.17), which we know should be cancelled by higher order discontinuities taken through the Reggeons themselves (see section 8.2). But if we overlook this difficulty, then a fixed-pole input in (11.4.4), i.e.

$$\gamma^2(t)\, R(t,s) \approx \gamma^2(t)\, s^{\alpha_0} \tag{11.4.9}$$

gives

$$D_2(s,t) = \bar{\beta}(t)\, s^{2\alpha_0 - 1} \tag{11.4.10}$$

where

$$\bar{\beta}(t) \equiv \frac{1}{16\pi^2} \iint_{-\infty}^0 \frac{\mathrm{d}t_1\, \mathrm{d}t_1'\, \theta(\lambda)}{(-\lambda(t,t_1,t_1'))^{\frac{1}{2}}}\, \gamma^2(t_1)\, \gamma^2(t_1') \tag{11.4.11}$$

and so from (11.4.7) and (2.7.2) with $\beta(t) \equiv \bar{\beta}/16\pi^2$

$$A_2(J,t) = \frac{\beta(t)}{J - (2\alpha_0 - 1)} \tag{11.4.12}$$

which in (11.4.8) gives

$$A(J,t) = \frac{\beta(t)}{J - (2\alpha_0 - 1) - \beta(t)} \tag{11.4.13}$$
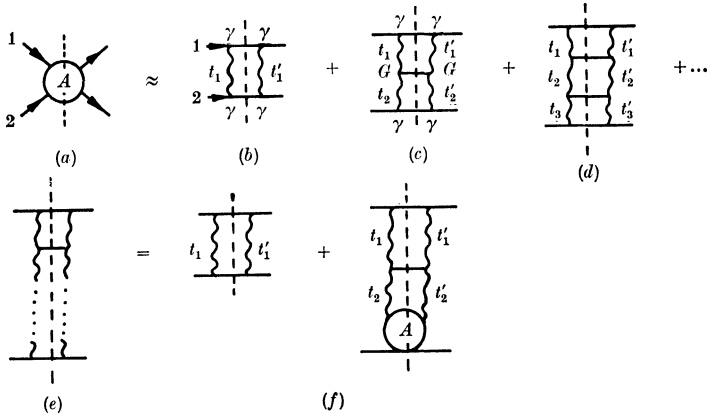
FIG. 11.12    The $s$-discontinuity of the amplitude $(a)$ is expressed in the multi-Regge approximation $(b)$–$(e)$. This is rewritten recursively in $(f)$.

i.e. a moving pole at

$$J = \alpha(t) \equiv 2\alpha_0 - 1 + \beta(t) \tag{11.4.14}$$

Note that if $\alpha_0 = 0$ this becomes $\alpha(t) = -1 + \beta(t)$ in accord with the field-theory result (3.4.19).

So unitarity replaces the input fixed cut (11.4.10) by a moving pole. Self-consistency of input and output at $t = 0$ (the dominant region of (11.4.11) if $\gamma(t)$ falls rapidly with $-t$) demands that

$$\alpha_0 = \alpha(0) = 2\alpha_0 - 1 + \beta(0), \quad \text{i.e.} \quad \alpha_0 = 1 - \beta(0) \tag{11.4.15}$$

so $\alpha(0) < 1$ in agreement with (11.4.3).

If alternatively we try a moving-pole input

$$\gamma^2(t)\, R(t,s) \approx \gamma^2(t)\, s^{\alpha(t)} \tag{11.4.16}$$

then from (8.2.17)

$$D_2(s,t) = \bar{\beta}(t) \frac{s^{\alpha_c(t)}}{\log s} \quad \text{where} \quad \alpha_c(t) \equiv 2\alpha\left(\frac{t}{4}\right) - 1 \tag{11.4.17}$$

giving, through (2.7.4),

$$A_2(J,t) = \beta(t) \log\left(J - \alpha_c(t)\right) \tag{11.4.18}$$

and so

$$A(J,t) = \frac{\beta(t) \log\left(J - \alpha_c(t)\right)}{1 - \beta(t) \log\left(J - \alpha_c(t)\right)} \tag{11.4.19}$$

So the output is an AFS cut which has moved from its original position at $J = \alpha_c(t)$, so again self-consistency is not achieved.

The problem is presumably due, at least in part, to the fact that to get even a crudely correct description of the scattering amplitude

we need to include both the Pomeron, P, and the secondary Reggeons R. For example, if we regard (11.4.9) as an approximation to the Reggeon input, $\alpha_0 = \alpha_R(0)$, then (11.4.14) can be regarded as the first approximation to the P. Then if both this fixed pole and (11.4.13) are inserted into $A_2$ in (11.4.8) we get also an AFS cut generated by the P, which must also be included, and so on. The final, self-consistent solution has a leading trajectory of the form

$$\alpha_P(t) = \alpha_R(t) + F(t) \log (\alpha_P(t) - \alpha_c(t)) \qquad (11.4.20)$$

where $\alpha_R(t)$ is the secondary Reggeon, and $\alpha_c(t) \equiv 2\alpha_P(t/4) - 1$ is the P $\otimes$ P cut. To satisfy this equation we must have

$$\alpha'_P(0) < \alpha'_R(0), \quad \alpha_R(0) < \alpha_P(0) < 1 \qquad (11.4.21)$$

(otherwise $\alpha_c(0) > \alpha_P(0)$). The properties of $\alpha_P(t)$ in (11.4.20) are very different for $t > 0$ and $t < 0$, and it has been called the 'schizophrenic Pomeron' by Chew and Snider (1971).

However, since cross-sections are found still to be rising at high energies this sort of solution of the Pomeron self-consistency problem no longer seems so attractive. Many variants of this approach have been suggested, but quite apart from their computational complexity, which generally necessitates over-simplification of the phase-space integrations, there seem to be two crucial difficulties. One is the generation of AFS cuts, which we know from section 8.2 would not be present if the $s$-discontinuities of the Reggeons themselves were also incorporated, and the other is the necessity for the strong-ordering assumption, which ensures that only planar diagrams are included. But since low sub-energies generally give the most important contributions to the integrals this is implausible, especially since we know that non-planar diagrams are essential if the correct Regge cut structure is to be obtained as well (see Halliday 1969).

## 11.5  The generating function

A very useful way of discussing the correlations in models of this sort is the generating function method of Mueller (1971).

In analogy with statistical mechanics the generating function or 'partition function' $Q(z, Y)$ is defined by

$$Q(z, Y) \equiv \sum_{n=0}^{\infty} z^n \sigma_{n+2}(Y) \qquad (11.5.1)$$

where $\sigma_{n+2}(Y)$ is the cross-section for producing $n$ particles (so that there are $n+2$ in the final state) at a given $Y \equiv \log(s/m_1 m_2)$ (which gives the length of the rapidity plot), and $z$ is an arbitrary parameter.

Clearly the point $z = 1$ has special significance in that

$$Q(1, Y) = \sum_n \sigma_{n+2}(Y) = \sigma_{12}^{\text{tot}}(Y) \qquad (11.5.2)$$

$$\left(\frac{\mathrm{d}Q}{\mathrm{d}z}\right)_{z=1} = \sum_n n\sigma_{n+2}(Y) = \langle n \rangle \sigma_{12}^{\text{tot}}(Y) = F_1 \sigma_{12}^{\text{tot}} \qquad (11.5.3)$$

$$\left(\frac{\mathrm{d}^2 Q}{\mathrm{d}z^2}\right)_{z=1} = \sum_n n(n-1)\,\sigma_{n+2}(Y) = \langle n(n-1) \rangle \sigma_{12}^{\text{tot}}(Y) = F_2 \sigma_{12}^{\text{tot}} \tag{11.5.4}$$

etc., using (10.3.11) and (10.3.16). So the behaviour of $Q$ in the neighbourhood of $z = 1$ gives average multiplicity of produced particles, and we can rewrite (11.5.1) as

$$Q(z, Y) = \sigma_{12}^{\text{tot}}(Y) \sum_{n=0}^{\infty} F_n(Y) \frac{(z-1)^n}{n!} \qquad (11.5.5)$$

(we define $F_0 \equiv 1$).

Also by differentiating (11.5.1) with respect to $z$ $n$ times and then setting $z = 0$

$$\sigma_{n+2}(Y) = \frac{1}{n!}\left(\frac{\mathrm{d}^n Q(z, Y)}{\mathrm{d}z^n}\right)_{z=0} \qquad (11.5.6)$$

so (11.5.1) can be regarded as a Taylor series for $Q(z, Y)$ about $z = 0$. Hence $z = 0$ is also a special point in that the behaviour of $Q$ in this neighbourhood gives all the multi-particle cross-sections.

Another useful set of relations is obtained by taking

$$\log(Q(z, Y)) = \log\left(\sum_n z^n \sigma_{n+2}(Y)\right) \qquad (11.5.7)$$

since
$$\left(\frac{\mathrm{d}(\log Q)}{\mathrm{d}z}\right)_{z=1} = \frac{1}{Q}\left(\frac{\mathrm{d}Q}{\mathrm{d}z}\right)_{z=1} = \left.\frac{\sum_n n z^{n-1}\sigma_{n+2}}{\sum_n z^n \sigma_{n+2}}\right|_{z=1}$$

$$= \frac{\sum_n n\sigma_{n+2}}{\sum \sigma_{n+2}} = \langle n \rangle = F_1 = C_1 \qquad (11.5.8)$$

$$\left(\frac{\mathrm{d}^2(\log Q)}{\mathrm{d}z^2}\right)_{z=1} = \left[-\frac{1}{Q^2}\left(\frac{\mathrm{d}Q}{\mathrm{d}z}\right)^2 + \frac{1}{Q}\left(\frac{\mathrm{d}^2 Q}{\mathrm{d}z^2}\right)\right]_{z=1}$$

$$= -\frac{\left(\sum_n n\sigma_{n+2}\right)^2}{\left(\sum_n \sigma_{n+2}\right)^2} + \frac{\sum_n n(n-1)\,\sigma_{n+2}}{\sum_n \sigma_{n+2}}$$

$$= -\langle n \rangle^2 + \langle n(n-1) \rangle = C_2(s) \qquad (11.5.9)$$

and in general

$$\left(\frac{\mathrm{d}^m(\log Q)}{\mathrm{d}z^m}\right)_{z=1} = C_m(s) \tag{11.5.10}$$

So $Q(z, Y)$ also gives directly all the correlation coefficients, and provides a simple way of deducing the $C$'s from the $\sigma_n$'s and vice versa.

A trivial example is provided by the multi-peripheral model, from which we expect no correlations because each particle is emitted independently. From (11.3.32)

$$\sigma_{n+2} = \bar{g}^4 \frac{(\bar{g}^2 Y)^n}{n!} \mathrm{e}^{-\bar{g}^2 Y} \tag{11.5.11}$$

and so (11.5.1) gives

$$Q(z, Y) = \bar{g}^4 \mathrm{e}^{-\bar{g}^2 Y} \sum_n \frac{z^n (\bar{g}^2 Y)^n}{n!} = \bar{g}^4 \mathrm{e}^{\bar{g}^2 Y(z-1)} \tag{11.5.12}$$

Hence, in agreement with (11.3.33),

$$\langle n \rangle = \left(\frac{\mathrm{d}(\log Q)}{\mathrm{d}z}\right)_{z=1} = \bar{g}^2 Y \tag{11.5.13}$$

but

$$C_2 = \left(\frac{\mathrm{d}^2(\log Q)}{\mathrm{d}z^2}\right)_{z=1} = \left[-\frac{1}{Q^2}\left(\frac{\mathrm{d}Q}{\mathrm{d}z}\right)^2 + \frac{1}{Q}\left(\frac{\mathrm{d}^2Q}{\mathrm{d}z^2}\right)\right]_{z=1} = 0 \tag{11.5.14}$$

and similarly all the other $C_m$ are zero because of the factorization built into the model.

More generally, if there are only short-range correlations we can expect all the $C$'s to increase like $\log s$, since for example if $c_2(y_3, y_4, s)$ in (10.10.1) vanishes for $|y_3 - y_4| > \Lambda$ (the correlation length), then the integral in (10.10.3) will be proportional to the length of the rapidity plot. This implies that we can write

$$\log(Q(z, Y)) = P(z) Y + S(z) \tag{11.5.15}$$

where $P$, $S$ are polynomials in $z$. The multi-peripheral model has, from (11.5.12),

$$P(z) = \bar{g}^2(z - 1), \quad S(z) = \log \bar{g}^4 \tag{11.5.16}$$

This expression (11.5.15) is reminiscent of the statistical mechanics of a gas (see Harari 1974). The grand partition function, $Q$, is related to the Helmholtz free energy, $A$, by

$$A = kT \log Q \tag{11.5.17}$$

This Helmholtz energy can be expressed as the sum of the volume energy $PV$ and the surface energy $S$, i.e.

$$A = PV + S = kT \log Q \tag{11.5.18}$$

and

$$P = kT \, \partial/\partial V (\log Q) \tag{11.5.19}$$

Now if we regard the rapidity plot (e.g. fig. 11.10) as representing a one-dimensional 'gas' in a container of length $V = Y$, the walls of the container being defined by the rapidities of the incoming particles, then (11.5.18) can be identified with (11.5.15) (if the energies are measured in units such that $kT = 1$). The statistical mechanics result (11.5.18) assumes that there are only short-range correlations between the motions of the gas molecules, due to short-range interactions both between the different molecules and between the molecules and the walls of the container, so that $\log Q \propto V$ as $V \to \infty$.

Of course the applicability of these statistical ideas at present energies is rather doubtful because even at CERN-ISR

$$\log s_{\max} \approx Y_{\max} = 8,$$

and we have seen that the correlation length is $\Lambda \approx 2$ (see (10.10.23)). We would hardly feel justified in employing the methods of statistical mechanics for a gas in a container whose length was only four times the range of the inter-molecular forces. But, as we shall see below, the generating-function method is a useful technique for calculating the correlations, etc., to be expected from various models.

## 11.6 The two-component model

We have found that though both the diffraction and multi-peripheral models have many features in accord with nature, neither is able to account for all the facts. This is not really surprising because we have seen that duality gives the Pomeron, P, which accounts for diffractive scattering in Regge language, a quite different status from that of the other Reggeons, R. And indeed, two-component duality, in which one adds the P and R contributions, was found to work quite well not only in two-body scattering (chapter 7) but also for the inclusive distributions (chapter 10). It seems likely, therefore, that models in which one adds diffractive and multi-peripheral components may be fairly successful in reproducing many-particle cross-sections (Harari and Rabinovici (1973), Fialkowski and Miettinen (1973); see Harari (1974) for a review). The obvious problems to be overcome are those of multiple counting in absorptive effects, and the inconsistency of multiple Pomeron exchange (see section 8.6).

We assume that the multi-peripheral component of the $2 \to n$ amplitude, $R_n$, is given by multiple R exchange (fig. 11.11) and so
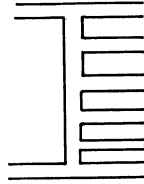
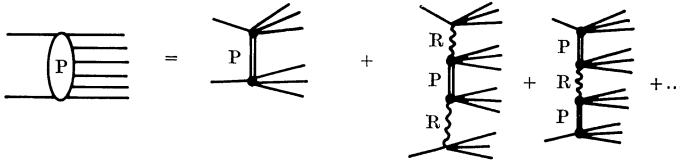FIG. 11.13    Duality diagram for a multi-peripheral R-exchange amplitude.



FIG. 11.14    Some of the contributions to the diffractive, P exchange, multi-peripheral amplitude. Terms with P and R or many P exchanges are all included in the diffractive component.

from (11.3.29) gives a contribution to the cross-section

$$\sigma_n^{\mathrm{R}} \sim s^{2\alpha_{\mathrm{R}}-2} \qquad (11.6.1)$$

(modulo $\log s$ factors) where $\alpha_{\mathrm{R}}$ is the leading non-Pomeron trajectory, so $\alpha_{\mathrm{R}}(0) \approx 0.5$. The duality diagram for this term is shown in fig. 11.13.

The diffractive component, $P_n$, will contain many different types of contribution depending on how many P exchanges occur, and where (fig. 11.14), and should give

$$\sigma_n^{\mathrm{P}} \sim \text{constant (modulo } \log s) \qquad (11.6.2)$$

The two-component hypothesis for the $2 \to n$ amplitude is that

$$A^{2 \to n} = R_n + P_n \qquad (11.6.3)$$

and so the $n$-body cross-section is symbolically, from (11.3.14),

$$\sigma_n = \frac{1}{s^2} \int \mathrm{d}\Phi_n'(|R_n|^2 + |P_n|^2 + 2\,\mathrm{Re}\,\{R_n P_n^*\})$$

$$\equiv \frac{1}{s^2}(R_n^2 + P_n^2 + R_n \cdot P_n) \qquad (11.6.4)$$

say, where multiplication implies integration over the $n$-body phase space, and we have introduced $\mathrm{d}\Phi_n' \equiv \mathrm{d}\Phi_n s/2$; see (11.3.26).

For the elastic $2 \to 2$ amplitude we have

$$\mathrm{Im}\,\{A^{\mathrm{el}}\} = \mathrm{Im}\,\{P_2 + R_2\} \qquad (11.6.5)$$

and so from the optical theorem (1.9.6) we obtain the consistency (bootstrap) condition that since

$$\sigma^{\text{tot}} = \frac{1}{s} \operatorname{Im} \{A^{\text{el}}\} = \sum_n \sigma_n$$

we must have

$$\frac{1}{s} \operatorname{Im} \{P_2 + R_2\} = \sum_n \frac{1}{s^2} \{R_n^2 + P_n^2 + P_n . R_n\} \qquad (11.6.6)$$

Now asymptotically $P_2 \sim s$, $R_2 \sim s^{\alpha_{\text{R}}}$ while $R_n^2 \sim s^{2\alpha_{\text{R}}}$, $P_n^2 \sim s^2$ and $R_n . P_n \sim s^{\alpha_{\text{R}}+1}$ (all modulo $\log s$) but of course we cannot be sure how $\sum_n$ of the right-hand side of (11.6.6) will behave. It seems fairly certain that part of $\operatorname{Im} \{P_2\}$ must come from $\sum_n P_n^2$ and part of $\operatorname{Im} \{R_2\}$ from $\sum_n R_n^2$, but we have seen how in the multi-peripheral model (11.3.30)

$$\frac{1}{s^2} \sum_n R_n^2 \sim s^{2\alpha_{\text{R}}-2+\bar{g}^2} \qquad (11.6.7)$$

so if $\bar{g}^2$ is large enough (i.e. $\bar{g}^2 = 1$ if $\alpha_{\text{R}} = 0.5$) this may also contribute to $P_2$. In fact it seems likely that this will be a very important contribution because the bulk of the multi-particle cross-section consists of particles with small sub-energies $(s_{i,i+1} < 2\,\text{GeV}^2)$ where in $2 \to 2$ scattering R exchange is much bigger than P exchange.

So if we consider processes like $pp \to pp + n(\pi^+\pi^-)$, which will contribute most of the inelastic charged-particle pp events, we can write

$$\sigma_n^{\text{inel}} \approx \frac{1}{s^2} (P_n^2 + R_n^2) \equiv \sigma_n^{\text{P}} + \sigma_n^{\text{R}} \qquad (11.6.8)$$

if we drop the interference term $P_n . R_n$. This may be justified on the grounds that $R$ contributes mainly to large multiplicities which populate evenly the whole of the rapidity plot (like fig. 11.6($d$)) while $P_n$ gives mainly low multiplicity events in the fragmentation region (fig. 11.6($a$), ($b$), ($c$)), so the overlap of the two types of events in the integral (11.6.4) is probably quite small. The relative magnitudes of the two terms will be denoted by $p$ and $r$ respectively, defined by

$$\sum_n \sigma_n^{\text{R}} = r\sigma^{\text{inel}} \quad \text{and} \quad \sum_n \sigma_n^{\text{P}} = p\sigma^{\text{inel}} \qquad (11.6.9)$$

so clearly

$$r + p = 1$$

The multiplicities provided by the two components are defined as

$$\langle n \rangle_{\text{R}} \equiv \frac{\sum_n n\sigma_n^{\text{R}}}{\sum_n \sigma_n^{\text{R}}} = \frac{\sum_n n\sigma_n^{\text{R}}}{r\sigma^{\text{inel}}}, \quad \langle n \rangle_{\text{P}} = \frac{\sum_n n\sigma_n^{\text{P}}}{\sum_n \sigma_n^{\text{P}}} = \frac{\sum_n n\sigma_n^{\text{P}}}{p\sigma^{\text{inel}}} \qquad (11.6.10)$$

and so, from (10.3.8), the average pion multiplicity is

$$\langle n \rangle = p \langle n \rangle_{\mathrm{P}} + r \langle n \rangle_{\mathrm{R}} \qquad (11.6.11)$$

i.e. just the weighted average of the multiplicities of the components. Similarly the correlations associated with each term are defined by (see (10.10.3))

$$\left. \begin{aligned} C_{2\mathrm{P}} &= \langle n(n-1) \rangle_{\mathrm{P}} - \langle n \rangle_{\mathrm{P}}^2 = \frac{\sum\limits_n n(n-1)\,\sigma_n^{\mathrm{P}}}{p\sigma^{\mathrm{inel}}} \\[2mm] C_{2\mathrm{R}} &= \langle n(n-1) \rangle_{\mathrm{R}} - \langle n \rangle_{\mathrm{R}}^2 = \frac{\sum\limits_n n(n-1)\,\sigma_n^{\mathrm{R}}}{r\sigma^{\mathrm{inel}}} \end{aligned} \right\} \qquad (11.6.12)$$

giving
$$C_2 \equiv \frac{\sum\limits_n n(n-1)\,(\sigma_n^{\mathrm{P}} + \sigma_n^{\mathrm{R}})}{\sigma^{\mathrm{inel}}} - \left( \frac{\sum\limits_n n(\sigma_n^{\mathrm{P}} + \sigma_n^{\mathrm{R}})}{\sigma^{\mathrm{inel}}} \right)^2$$

$$= pC_{2\mathrm{P}} + rC_{2\mathrm{R}} + p\langle n \rangle_{\mathrm{P}}^2 + r\langle n \rangle_{\mathrm{R}}^2 - (p\langle n \rangle_{\mathrm{P}} + r\langle n \rangle_{\mathrm{R}})^2$$

$$= pC_{2\mathrm{P}} + rC_{2\mathrm{R}} + rp(\langle n \rangle_{\mathrm{P}} - \langle n \rangle_{\mathrm{R}})^2 \qquad (11.6.13)$$

(using $r + p = 1$) which is not the weighted average of (11.6.12). This is a rather important result, because even if $C_{2\mathrm{P}} \sim$ constant, and $C_{2\mathrm{R}} = 0$ (equation (11.5.14)), we shall still get $C_2 \sim \log^2 s$, implying some long-range correlations, provided $\langle n \rangle_{\mathrm{R}} \sim \log s$ as expected from (11.3.33), and this is in much better accord with the data in fig. 10.29. The long-range correlations arise just because we have the sum of two types of exchanges, P and R, so factorization does not hold.

Harari and Rabinovici (1972) (see also Harari (1974)) have fitted the pp data with a model of this sort, assuming that $\sigma_n^{\mathrm{P}} = d_n$ are constants for $n = 0, 1, 2$ (i.e. for 2, 4, 6 prongs) and $\sigma_n^{\mathrm{P}} = 0$ for $n > 3$ (i.e. the diffractive component contributes only to the lowest multiplicities), while $\langle n \rangle_{\mathrm{R}} = c_1 \log(s/s_1)$ and $C_{2\mathrm{R}} = c_2 \log(s/s_2)$, $C_{m\mathrm{R}} = 0$ for $m > 2$. The seven parameters $d, d_1, d_2, c_1, c_2, s_1, s_2$ enable them to fit $\langle n \rangle$, $C_2$ and $\sigma_n$, $0 \leqslant n \leqslant 6$.

From (11.6.9)
$$p = \frac{d_0 + d_1 + d_2}{\sigma^{\mathrm{inel}}} \qquad (11.6.14)$$

They find $p = 0.16$, so the multi-peripheral component dominates, as is rather clear from the fall of the multiplicity cross-sections in fig. 11.15. Also from (11.6.11)

$$\langle n \rangle = rc_1 \log\left(\frac{s}{s_1}\right) + \frac{d_1 + 2d_2}{\sigma^{\mathrm{inel}}} \to rc_1 \log\left(\frac{s}{s_1}\right) \qquad (11.6.15)$$
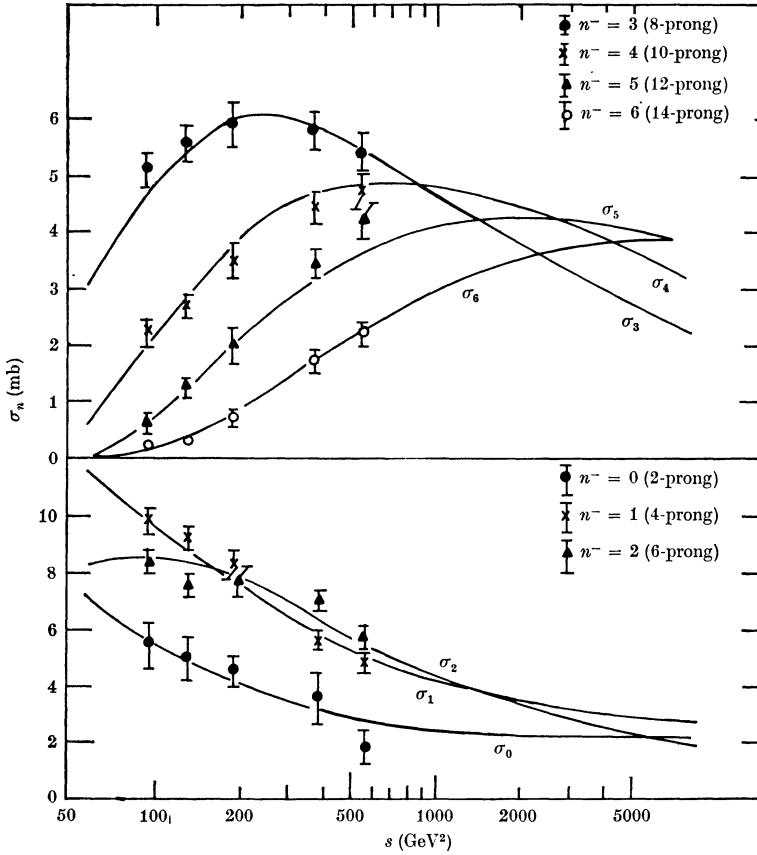
FIG. 11.15   Fit to the energy dependence of the multiplicity cross-sections in pp → pp + n(π⁺π⁻) with the two-component model (from Harari 1974).

and from (11.6.13)

$$C_2 = rpc_1^2 \left( \log \left( \frac{s}{s_1} \right) \right)^2 + rc_2 \log \left( \frac{s}{s_2} \right) - 2r \left( \frac{d_1 + 2d_2}{\sigma} \right) \log \left( \frac{s}{s_1} \right)$$

$$+ pC_{2\mathrm{P}} + rp\langle n \rangle_{\mathrm{P}}^2 \to rpc_1^2 \left( \log \left( \frac{s}{s_1} \right) \right)^2 \quad (11.6.16)$$

So the two-component model gives

$$\frac{C_2}{\langle n \rangle^2} \to \frac{p}{r} = \text{constant} \qquad (11.6.17)$$

which is experimentally quite good, and certainly much better than $C_2/\langle n \rangle^2 \sim (\log s)^{-1}$ from the multi-peripheral type of model, or $\sim (\sqrt{s}) (\log s)^{-2}$ from the diffraction model ((11.2.17), (11.2.19)).

From (11.5.1) and (11.5.5)

$$Q_R(z, Y) = r\sigma^{\text{inel}} \exp\left\{\sum_i [(z-1)^i/i!] C_{iR}\right\}$$

$$= r\sigma^{\text{inel}} e^{(z-1)\langle n\rangle_R + \frac{1}{2}(z-1)^2 C_{2R}} \sim s^{-c_1 + \frac{1}{2}c_2} \quad \text{at} \quad z = 0 \quad (11.6.18)$$

and since (from (11.5.6))

$$\sigma_n^R = \frac{1}{n!}\left(\frac{\mathrm{d}^n Q_R(z, Y)}{\mathrm{d}z^n}\right)_{z=0} \tag{11.6.19}$$

all

$$\sigma_n^R \sim s^{-c_1 + \frac{1}{2}c_2} \tag{11.6.20}$$

With (11.6.1) this gives $2\alpha_R - 2 = -c_1 + \frac{1}{2}c_2$, and the parameters required to fit the data ($c_1 = 1.0$, $c_2 = 0.35$) give $\alpha_R = 0.59$, in reasonable agreement with expectation.

Since from (11.6.8) and (11.3.40)

$$\sigma_n^{\text{inel}} = \sigma_n^P + \sigma_n^R$$

$$= d_n + r\sigma^{\text{inel}} \frac{e^{-\langle n\rangle}\langle n\rangle^n}{n!} \tag{11.6.21}$$

the two-component model predicts a multiplicity distribution like fig. 11.16, with a dip developing at high $\log s$ as the peak of the multiperipheral part moves out. However, we have, *inter alia*, neglected the likely $\log s$ dependence of the $d_n$ which may destroy this conclusion. If successive P exchanges are permitted in $\sigma_n^P$ such logarithmic increases are bound to occur (see for example (10.8.20)), but because the triple-P coupling is small this may only be a small effect. It all depends on how one tries to solve the self-consistency problem of the $P_n$ part of (11.6.6) – with $\alpha_P(0) < 1$ as in (11.4.3), $= 1$ as in (8.6.9), or $> 1$ as in (8.6.14), which all give different behaviours for $\sigma^{\text{tot}}(s)$.

But if we are willing to push such problems to the back of our minds, this sort of two-component model seems to provide rather a good first approximation of the data.


## 11.7   The duality bootstrap

The two-component model, which combines the virtues of the diffraction and multi-peripheral models, and two-component duality, seems to be along the right lines. However, it clearly does not make full use of the content of duality as discussed in sections 7.3 and 10.7. Nor can it be regarded as self-consistent in that both multiple-P exchange and the planar nature of the multi-peripheral model are inconsistent
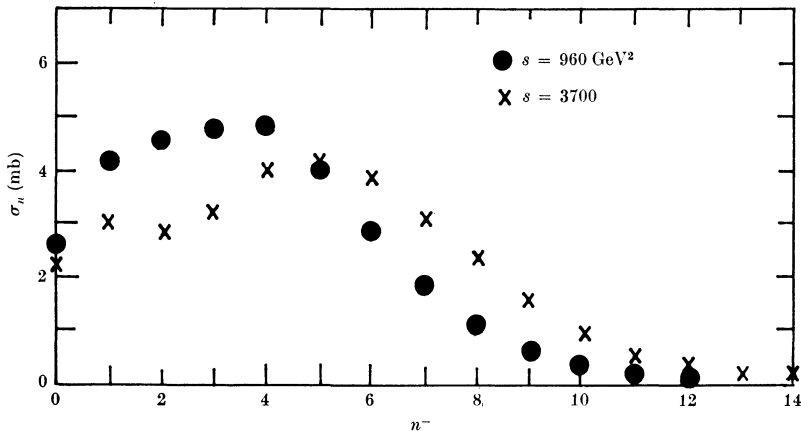
FIG. 11.16   Predictions of the two-component-model fit for the high
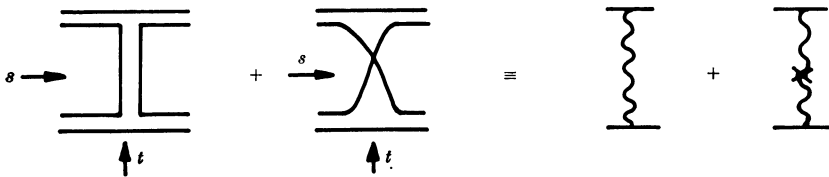energy multiplicity distributions (from Harari 1974).



Fig. 11.17   The $s$–$t$ and $t$–$u$ planar duality diagrams which provide the
two contributions to the signature factor of a $t$-channel Reggeon.

with unitarity requirements. Recently some progress has been made
in overcoming these problems by making better use of duality (Lee
1973, Veneziano 1973, 1974$b$, Chan, Paton and Tsou 1975, Aurenche
$et\ al.$ 1975).

In $2 \rightarrow 2$ scattering there are just two diagrams for R exchange in
the $t$ channel (see figs. 11.17), one $s$–$t$ planar, the other $t$–$u$ planar,
which give the two discontinuities ($s$- and $u$-channel) of a definite-
signature Reggeon. Then in $2 \rightarrow 3$ we have the four diagrams of
figs. 11.18, and so on, there being $2^{n-1}$ different diagrams for an
$n$-particle final state. Only one of these is $s$–$t$ planar, and all the other
$2^{n-1} - 1$ are non-planar, but all the diagrams contribute equally to $\sigma_n$,
and so, like (11.3.29),

$$\sigma_n = 2^{n-1} \bar{g}^4 \frac{(\bar{g}^2 Y)^{n-2}}{(n-2)!} s^{2\alpha_{\mathrm{R}}-2} \tag{11.7.1}$$

if we neglect interference between the various terms.

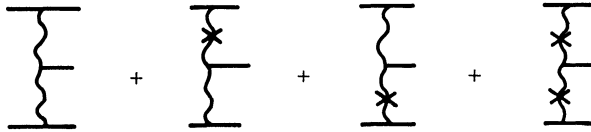However, the crossed diagram in fig. 11.19$(a)$ does not contribute

FIG. 11.18    The four different signature contributions
to the $2 \to 3$ double-Regge amplitude.

to $\sigma^{\text{tot}}$ because it does not contribute to $\text{Im}\{A^{2\to 2}\}$ for $s > 0$, only for $s < 0$. From (11.6.6) we have

$$\text{Im}\{A^{2\to 2}\} = \text{Im}\{R_2 + P_2\} \qquad (11.7.2)$$

$$= \sum_{n=2}^{\infty} A^{2\to n} A^{*2\to n} \qquad (11.7.3)$$

which is represented by fig. 11.19(b) (where again we have neglected cross terms like fig. 11.19(c), see (11.6.8) *et seq.*). Only the first diagram in each group is planar, and so can contribute to R, and so all the other non-planar ones presumably build up P. Hence

$$\sigma^{\text{tot}}(s) = \frac{1}{s}\text{Im}\{A^{2\to 2}\} = \frac{1}{s}\text{Im}\{R_2 + P_2\} \qquad (11.7.4)$$

$$= \sum_n \sigma_n = \sum_n 2^{n-1}\bar{g}^4 \frac{(\bar{g}^2 Y)^{n-2}}{(n-2)!} s^{2\alpha_{\text{R}}-2} \qquad (11.7.5)$$

but for each $n$ only 1 term contributes to R and $(2^{n-1} - 1)$ to P, so

$$\frac{1}{s}\text{Im}\{R_2\} \sim s^{\alpha_{\text{R}}-1} = \sum_n \bar{g}^4 \frac{(\bar{g}^2 Y)^{n-2}}{(n-2)!} s^{2\alpha_{\text{R}}-2} \sim s^{2\alpha_{\text{R}}-2+\bar{g}^2} \qquad (11.7.6)$$

$$\frac{1}{s}\text{Im}\{P_2\} \sim s^{\alpha_{\text{P}}-1} = \sum_n (2^{n-1} - 1)\bar{g}^4 \frac{(\bar{g}^2 Y)^{n-2}}{(n-2)!} s^{2\alpha_{\text{R}}-2} \sim s^{2\alpha_{\text{R}}-2+2\bar{g}^2} \qquad (11.7.7)$$

so $\qquad\qquad \alpha_{\text{R}} = 1 - \bar{g}^2, \quad \alpha_{\text{P}} = 2\alpha_{\text{R}} - 1 + 2\bar{g}^2 = 1 \qquad (11.7.8)$

Thus, unlike (3.4.13), (11.3.30) and (11.4.14), the height of the trajectory $\alpha_{\text{R}}$ decreases as the strength of the coupling, $\bar{g}^2$, increases, and, even more remarkably, $\alpha_{\text{P}} = 1$ independent of the coupling strength.

Much more detailed calculations along these lines have been attempted by Chan and co-workers (Aurenche *et al.* 1975). For each $A^{2\to n}$ they use a dual amplitude, but for small sub-energies $s_{i,i+1} < \bar{s}$, say, they approximate the dual amplitude by its resonance contributions in the $s_{i,i+1}$ channel, while for $s_{i,i+1} > \bar{s}$ they use the Regge
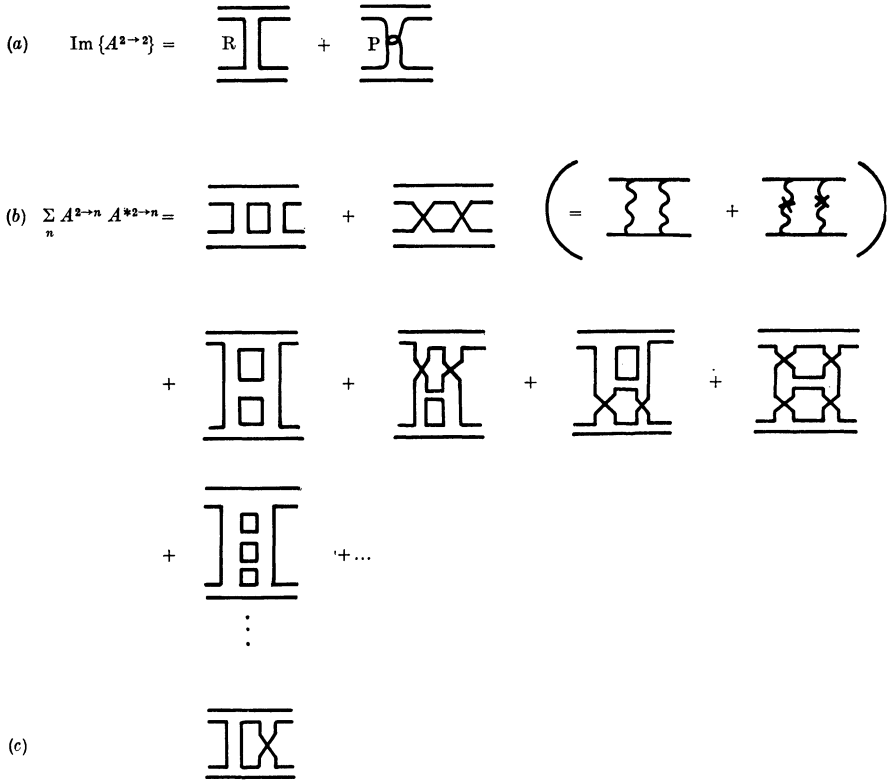
FIG. 11.19 (a) R+P contributions to Im $\{A^{2\to2}\}$. (b) Duality diagrams for the multi-Regge contributions to $\sum_n A^{2\to n} A^{*2\to n}$. (c) A cross term of the type neglected in (b).

exchange approximation (see fig. 11.20(a)). Also they include the SU($N$), $N = 2$ (or 3), symmetry by including $\tau$ (or $\lambda$) matrices for each quark, as we described when obtaining (9.4.26), which ensures $I = 0$ for the P, and degenerate $I = 0$, 1 trajectories for R etc. The structure naturally gives

$$\alpha_P(0) > \alpha_R(0), \quad \alpha'_P < \alpha'_R$$

They insert the Reggeon into integral equations like (11.4.6) (see fig. 11.21), perform loop integrations similar to (11.4.4), and insist that the output Reggeon be the same as the input. This gives the parameters of the P trajectory, which for $\alpha_R^0 = 0.5$, $\alpha'_R = 1$ input gives $\alpha_P^0 = 1.12$, $\alpha'_P = 0.1$ output, which are not too far from the observed values.
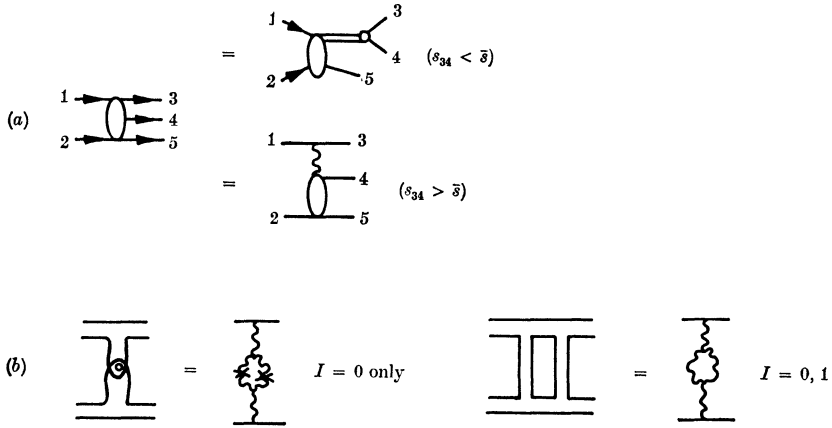
FIG. 11.20   (a) The amplitude for $12 \to 345$ is represented by resonance production for $s_{34} < \bar{s}$, and R exchange for $s_{34} > \bar{s}$. (b) The P with $I = 0$ only generated by a 'twisted' loop, and R with $I = 0$ or $1$ generated by an untwisted loop.
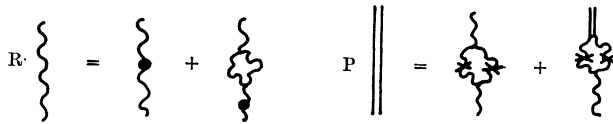


FIG. 11.21   Schematic representation of the integral equations used by Aurenche *et al.* (1975) to generate R and P contributions. For lines with round blobs only $s < \bar{s}$ (i.e. the input resonance contribution) is included since for $s > \bar{s}$ the resonances are equivalent to R exchange (cf. fig. 11.12 (f)).

But of course the next iteration with the P included in the input will produce cuts with $\alpha_c(0) > 1$, which brings us back to the problem which has featured several times in our discussion, how the P with $\alpha_{\mathrm{P}}(0) \approx 1$ can be made consistent with unitarity (see for example (11.3.31) *et seq.*). If $\alpha_{\mathrm{P}}(0) < 1$ there is, in principle, no problem, because at very high energies the self-consistent solution will look rather like the multi-peripheral bootstrap, with a single dominant P pole exchange and $\alpha_{\mathrm{P}}(0) = 1 - \bar{g}^2$ as in (11.4.3). The continuing rise of $\sigma^{\mathrm{tot}}(s)$ at CERN-ISR energies has to be regarded as a non-asymptotic effect, and eventually $\sigma^{\mathrm{tot}}(s) \to 0$ as $s \to \infty$. If $\alpha_{\mathrm{P}}(0) = 1$ then the pole cannot be dominant asymptotically unless the triple-P coupling $\gamma^{\mathrm{PP,P}}(t) \to 0$ as $t \to 0$ (see (10.8.21)) to forbid multi-Pomeron exchange, which phenomenologically seems untrue. So a self-consistent solution must have dominant cuts, as in the Reggeon field theory mentioned in section 8.3, and $\sigma^{\mathrm{tot}}(s) \sim (\log s)^\nu$, $\nu > 0$, and $\alpha_{\mathrm{P}}(t) = 1 + \alpha'(t)^\kappa$ (see

Abarbanel *et al.* 1975) so the trajectory is quite unlike fig. 6.6(*b*). Or if $\alpha_P(0) > 1$ we have cut dominance, and all the absorption problems discussed in section 8.6 occur not only for $P \otimes P$ cuts but for $R \otimes P$ as well, so the apparent dominance of poles at available energies becomes a non-asymptotic effect. In fact, as we noted in sections 8.3 and 10.8 these self-consistency problems require a consideration of what happens not just at large $\log s$, but large $\log(\log s)$, which is not achievable even in principle.

At present Regge poles seem to fit the data far better than one has any right to expect, which is pleasant for the phenomenologist. But it means that one can gain rather little insight from experiment as to the nature of the unitarity constraints which must inter-relate poles and cuts, and restrict the Reggeon parameters, and may even uniquely determine them in the full bootstrap sense. The models discussed in this chapter take us only a little way towards such a self-consistent unitarization, and although the incorporation of duality has produced a useful advance towards building up the Pomeron we are still as far as ever from understanding how it can be made consistent. The approach is still a perturbative one, except that the effective expansion parameter is $\gamma^{PP,P}(t) \log s$ (rather than the residue in, say, (11.3.20), see Chew (1973)) so that, since $\gamma^{PP,P}(0)$ is small, there is quite good convergence for small $\log s$, but the expansion will not converge for large $\log s$, and so we do not attain a self-consistent asymptotic behaviour.

These problems make it hard to understand why dual models, which are based on imposing the desired Regge asymptotic behaviour on non-unitarity narrow-resonance amplitudes, are so successful. In particular, what is the significance of the fact that they require, even in the Born approximation, linear trajectories $\alpha_B(t) = \alpha_B^0 + \alpha_B' t$, where $\alpha_B' \approx 1\,\mathrm{GeV}^{-2}$ sets the scale for hadronic interactions? If unitarity is to make only a small change in these trajectory functions ($\alpha(t) \approx \alpha_B(t)$ for all $t$) they must satisfy the twice subtracted dispersion relation (3.2.12) with $\mathrm{Im}\{\alpha\}$ small. However, the Regge trajectories which are generated by the iteration of a basic exchange force in some sort of ladder, as in potential scattering (section 3.3), field theory (section 3.4), or the Reggeized multi-peripheral model (section 11.3), all obey the singly subtracted dispersion relation (3.3.11), where $n$ is a constant which depends on the asymptotic behaviour of the Born approximation (see (3.3.32), (3.4.19)) but the position of the trajectory (and hence $\alpha'(t)$) depends on the coupling strength $g^2$ through unitarity,

and $\alpha' \to 0$ as $g^2 \to 0$. It has been suggested (see Veneziano 1974) that perhaps one should regard $\sqrt{\alpha'} \approx 2 \times 10^{-14}$ cm as a fundamental length, below which the concept of point-like particles does not make any sense. But if $\alpha_B'^{-1}$ is the fundamental energy scale of hadronic physics it is hard to see how the trajectories can possibly be built up through unitarity as bootstrap models require (Collins *et al.* 1968*a*, Collins 1971).

Even more obscure is the relation between the quark model, which describes the internal symmetry structure of the dual Born approximation so well (for example in duality diagrams), and the dynamics of unitary models. The harmonic oscillator type of potential between quarks, which is needed to generate linear trajectories and reproduce the resonance spectrum (see section 3.3), and which must also prevent quarks from actually being produced in scattering experiments, is not evident in particle scattering at all. The forces between the particles (due to Reggeon exchange) seem quite different from the forces between the quarks, despite the fact that the particles are supposed to be composed of quarks. Various schemes for confining quarks in 'bags' have been proposed, but their significance for Regge dynamics is not yet clear (see Chados *et al.* 1974).

So we are still some way from understanding why Regge theory, and in particular Regge pole dominance, works so well, yet unitarization, which first motivated the introduction of Reggeons rather than fixed-spin elementary particles, seems comparatively unimportant. But at least it has become much clearer what are the relevant questions to ask about hadronic interactions, which gives us reason for anticipating that some of these fundamental questions may be solved before very long.